

**A Consistent Poleward Shift of the Storm Tracks
in Simulations of 21st Century Climate**

Jeffrey H. Yin

National Center for Atmospheric Research, Boulder, CO, USA

Submitted to *Geophysical Research Letters*

May 31, 2005

Revised August 12, 2005

Corresponding author:
Jeffrey H. Yin
National Center for Atmospheric Research
ESSL/Climate and Global Dynamics Division
P.O. Box 3000
Boulder, CO 80307-3000
Phone: 303-497-1379
Fax: 303-497-1333
Email: jyin@ucar.edu

Abstract

A consistent poleward and upward shift and intensification of the storm tracks is found in an ensemble of 21st century climate simulations performed by 15 coupled climate models. The shift of the storm tracks is accompanied by a poleward shift and upward expansion of the midlatitude baroclinic regions associated with enhanced warming in the tropical upper troposphere and increased tropopause height. The poleward shift in baroclinicity is augmented in the Southern Hemisphere and partially offset in the Northern Hemisphere by changes in the surface meridional temperature gradient. The poleward shift of the storm tracks also tends to be accompanied by poleward shifts in surface wind stress and precipitation, and a shift towards the high index state of the annular modes. These results highlight the integral role that the storm tracks play in the climate system, and the importance of understanding how and why they will change in the future.

1. Introduction

The storm tracks, defined as regions with large synoptic-scale baroclinic wave activity (Blackmon et al. 1977), play an important role in both weather and climate. From a synoptic point of view, baroclinic waves are the storms associated with much of the precipitation and severe weather in midlatitudes. From a climatic point of view, baroclinic waves in the storm tracks transport large amounts of heat, moisture, and momentum polewards, interact with the large-scale circulation to produce patterns of climate variability, and drive ocean circulation via wind stress resulting from their momentum flux convergences. From both perspectives, the response of the storm tracks to future climate change is of great interest.

Recent reanalysis-based studies indicate that there has been a poleward shift in the mean latitude of extratropical cyclones, and that cyclones have become fewer and more intense, over the last half of the 20th century (e.g., McCabe et al. 2001; Fyfe 2003). There has also been an increase in bandpass-filtered wind variance associated with the storm tracks (e.g., Chang and Fu 2002), although this trend may be exaggerated in reanalysis data (Harnik and Chang 2003). Since attribution of these observed trends to anthropogenic greenhouse gas (GHG) forcing is limited by the as-yet small GHG-forced signal relative to climate variability, it is useful to compare the observed changes in storm tracks with those simulated by general circulation models (GCMs) forced by increasing GHGs.

Previous GCM studies of GHG-forced storm track changes have produced some consistent results; for example, many have found that cyclones become fewer and more intense with increasing GHGs, as in observations (e.g., Lambert 1995; Geng and Sugi 2003). GCM experiments forced by increasing GHGs also tend to produce poleward

shifts and increases in intensity of the storm tracks as measured by bandpass-filtered variables (e.g., Hall et al. 1994; Kushner et al. 2001), although there are some exceptions, particularly in low-resolution GCMs (e.g., Stephenson and Held 1993). Each of these previous studies has examined the storm track response to increasing GHGs in just one GCM.

In this paper, we analyze the output of 15 coupled GCMs that have performed historical and future climate change experiments for the upcoming Intergovernmental Panel on Climate Change (IPCC) Fourth Assessment Report (AR4). The aim of this paper is to document the consistent poleward shift in the storm tracks seen in the IPCC AR4 simulations of 21st century climate, to relate this shift to changes in baroclinicity, and to illustrate the importance of these storm track changes for 21st century climate.

2. Model experiments

The model output analyzed here was archived by the Program for Climate Model Diagnosis and Intercomparison (<http://esg.llnl.gov:8443/index.jsp>), from which we downloaded the files. The horizontal resolution of the model output varied from 4° by 5° to spectral T106 (approximately 1.125° by 1.125°); the coupled GCMs used in this paper, in order from highest to lowest atmospheric resolution, are: MIROC3.2(hires), CCSM3, ECHAM5/MPI-OM, GFDL-CM2.0, GFDL-CM2.1, CNRM-CM3, MIROC3.2(medres), MRI-CGCM2.3.2, FGOALS-g1.0, IPSL-CM4, CGCM3.1(T47), ECHO-G, GISS-AOM, GISS-ER, and INM-CM3.0. Documentation for the models can be found at http://www-pcmdi.llnl.gov/ipcc/model_documentation/ipcc_model_documentation.php.

We compare the output from two of the IPCC AR4 experiments, which we refer to as 20C and A1B. Experiment 20C uses initial conditions from a preindustrial control run and is forced with historical GHG, aerosol, volcanic, and solar forcing from the 20th

century. Experiment A1B uses initial conditions from the end of experiment 20C and is forced with specified GHGs for the period 2001-2100 from scenario A1B of the IPCC Special Report on Emissions Scenarios (Nakicenovic and Swart 2000), with atmospheric CO₂ levels rising to approximately 720 ppm by 2100.

To represent the climate change during the 21st century, we compare 19 years from the end of the 21st century (September 2081-August 2100) in experiment A1B to 19 years from the end of experiment 20C (September 1981-August 2000). Due to the different years of model output saved, years 1980-1999 and 2080-2099 were used for CCSM3. While some models had more than one ensemble member for each experiment, we analyze output from the one ensemble member from each model for which daily mean output was saved.

3. Poleward shift of the storm tracks and baroclinicity

In this paper, we represent the storm tracks using eddy kinetic energy (EKE) that has been filtered to retain variability on synoptic time scales of 2-8 days. We begin by examining the consensus among the models as represented by the 15-member multi-model ensemble. The multi-model mean 2081-2100 minus 1981-2000 difference in zonal mean 2-8 day EKE for December-February (DJF) and June-August (JJA) is shown in Fig. 1. In response to 21st century climate change, the storm tracks shift poleward and upward and increase in magnitude in both hemispheres in DJF and in the Southern Hemisphere (SH) in JJA. The weak JJA Northern Hemisphere (NH) storm track also shifts poleward and upward, but it weakens slightly.

The poleward and upward shift of the storm tracks is related to changes in baroclinicity associated with the thermal structure of the troposphere. Figs. 2a-b show the multi-model mean 2081-2100 minus 1981-2000 difference in zonal mean

temperature. Note the warming in the tropical upper troposphere in DJF and JJA, due to a decrease in the moist adiabatic lapse rate as temperature increases; the warming near the surface in NH high latitudes in DJF, due to thinning and retreat of sea ice; and the relatively small warming near the surface in SH high latitudes, due to the large thermal inertia of the Southern Ocean. All three features are present in all models.

The baroclinicity is represented by the maximum Eady growth rate (Lindzen and Farrell 1980), calculated as $\sigma^{\text{BI}} = 0.31 g N^{-1} T^{-1} |\partial T/\partial y|$, where T is the zonal mean temperature and N is the Brunt-Vaisala frequency calculated using T . The changes in baroclinicity associated with multi-model mean changes in T between 2081-2100 and 1981-2000 are shown in Figs. 2c-d. The midlatitude baroclinic zones tend to expand upward in response to the higher tropopause; this may be related to the overall increase in EKE, since the deeper baroclinic zone contains more available potential energy to be tapped by baroclinic waves. Also note the clear poleward shift in baroclinicity throughout the troposphere in the SH, where near-surface changes in baroclinicity augment those in the upper troposphere; this is consistent with the poleward shift of EKE. In NH winter, the poleward shift in baroclinicity is partially offset by the reduction in high-latitude baroclinicity near the surface, which may be related to the smaller increase in EKE. The decrease in baroclinicity below 300 hPa in NH summer appears to dominate the increase in baroclinicity near the tropopause, as evidenced by the overall decrease in EKE.

The effect of temperature on baroclinicity can be divided into the effect of the meridional temperature gradient $|\partial T/\partial y|$, shown in Figs. 2e-f, and the effect of static stability N , shown in Figs. 2g-h. In a similar analysis, Geng and Sugi (2003) showed the changes in $|\partial T/\partial y|$ and N from a GHG warming experiment and concluded that the

changes in baroclinicity were mainly due to $|\partial T/\partial y|$ in the NH and N in the SH. However, the relative contributions of $|\partial T/\partial y|$ and N were not completely clear, because their respective effects on baroclinicity were not explicitly calculated. In Figs. 2e-h, the explicit calculation of the effects of $|\partial T/\partial y|$ and N on the maximum Eady growth rate shows that the effect of $|\partial T/\partial y|$ on baroclinicity is clearly larger. While the effect of increased N is to decrease baroclinicity throughout the troposphere, which is the dominant effect in NH summer, the poleward shift of baroclinicity found in all other seasons is primarily due to changes in $|\partial T/\partial y|$.

A preliminary analysis of the energy budget, using the methods of Trenberth and Stepaniak (2003), suggests that the poleward shift of baroclinicity is largely maintained by anomalous energy transports in the Ferrel cell, which shifts poleward in response to anomalous momentum fluxes in the storm tracks. Due to the feedback between the storm tracks and the zonal mean flow, the cause of the poleward shift cannot be sorted out by diagnostic analysis alone; this will require additional model experiments, perhaps using an idealized model (e.g., Lee and Kim 2003). For example, such a model could separately simulate the responses of the storm tracks to increased tropical latent heating and increased upper tropospheric $|\partial T/\partial y|$. The dynamics behind the consistent poleward shift of the storm tracks in response to increasing GHGs is left as a subject for future research.

How consistent is the poleward shift of the storm tracks? Figs. 3a-b show the change in the zonal mean of vertically integrated 2-8 day EKE for each of the 15 models. For the SH storm track, all models except INM-CM3.0 have a poleward shift in DJF, and all but three (FGOALS-g1.0, GISS-AOM, INM-CM3.0) also have a poleward shift in

JJA. All but four (ECHAM5/MPI-OM, MRI-CGCM2.3.2, GISS-AOM, INM-CM3.0) have a poleward shift of the NH storm track in DJF. The NH storm track in JJA primarily weakens in most models, although 9 of the 15 models produce a poleward shift as well. Thus, the multi-model ensemble means shown in Fig. 1 represent the consensus among the models; differences in storm track responses between the models will be examined elsewhere.

4. Connections with other climate variables

To illustrate the important role of the storm tracks in the climate system, we now examine the changes that accompany the poleward shift of the storm tracks. Figs. 3c-d show that the poleward shift of the storm track tends to be accompanied by a poleward shift in vertically integrated 2-8 day momentum flux convergence, which is expected to drive a similar shift in the midlatitude jets and surface zonal wind stress (e.g., Kushner et al. 2001). As shown in Figs. 3e-f, the maximum zonal wind stress does tend to shift poleward, with approximately half of the wind stress change explained by 2-8 day momentum flux convergence. The poleward shift of zonal wind stress is significant in light of the results of Russell et al. (2005) and Toggweiler et al. (2005), who have found that the location of the midlatitude surface westerlies is important for driving upwelling in the Southern Ocean, which may in turn control atmospheric CO₂ during the ice ages.

The storm tracks are intimately tied to patterns of climate variability, such as the NH and SH annular modes (NAM and SAM). Figs. 3g-h show that the poleward shift of the storm tracks tends to be accompanied by a reduction in sea level pressure (SLP) over the pole and an increase in SLP at lower latitudes, indicating a shift towards the high index state of the NAM and SAM. While the NAM and SAM are expressions of the internal variability of the atmosphere, they may be pushed toward one polarity by

external forcings such as stratospheric ozone depletion or GHG-forced warming (e.g., Arblaster and Meehl 2005).

The poleward shift of the storm tracks also tends to be accompanied by a poleward shift of midlatitude precipitation, as shown in Figs. 3i-j. This is less true in NH summer, when a larger fraction of the precipitation is associated with convection over land. The poleward shift of midlatitude precipitation is consistent with other analyses of precipitation in GCM simulations of GHG-forced climate change (e.g., Emori and Brown 2005; Meehl et al. 2005; Min et al. 2005). Future work will investigate the influence of the storm tracks on the statistics of extreme precipitation events.

5. Summary

We have documented the consistent poleward and upward shift and intensification of the storm tracks found in simulations of 21st century climate performed by 15 different coupled GCMs for the IPCC AR4. The poleward and upward shift of the storm tracks is accompanied by a poleward shift and upward expansion of the midlatitude baroclinic regions associated with enhanced warming in the tropical upper troposphere and increased tropopause height. The poleward shift in baroclinicity is augmented by the increased surface temperature gradient in the SH, and is partially offset by the reduced surface temperature gradient in NH winter. The poleward shift of the storm tracks tends to be accompanied by poleward shifts in surface wind stress and precipitation, and a shift towards the high index state of the NAM and SAM. While the mechanisms for the poleward shift of the storm tracks and the differences in the storm track response between GCMs remain under investigation, these results highlight the integral role that the storm tracks play in the climate system, and the importance of understanding how and why they will change in the future.

Acknowledgments

This work was supported by NOAA Cooperative Agreement No. NA17GP1376. The National Center for Atmospheric Research is supported by the National Science Foundation. I would like to thank J. Hurrell for advice on this work; G. Meehl and two anonymous reviewers for helpful comments on this manuscript; S. Emori, Z. Liu, C. Mitas, W. Robinson, E. Schneider, and Y. Tsushima for useful discussions; and S.-K. Min for providing output from the ECHO-G model. I acknowledge the international modeling groups for providing their data for analysis, the Program for Climate Model Diagnosis and Intercomparison (PCMDI) for collecting and archiving the model data, the JSC/CLIVAR Working Group on Coupled Modelling (WGCM) and their Coupled Model Intercomparison Project (CMIP) and Climate Simulation Panel for organizing the model data analysis activity, and the IPCC WG1 TSU for technical support. The IPCC Data Archive at Lawrence Livermore National Laboratory is supported by the Office of Science, U.S. Department of Energy.

References

- Arblaster, J. M., and G. A. Meehl, 2005: Contribution of various external forcings to trends in the Southern Annular Mode. Submitted to *J. Climate*.
- Blackmon, M. L., J. M. Wallace, N.-C. Lau, and S. L. Mullen, 1977: An observational study of the Northern Hemisphere wintertime circulation. *J. Atmos. Sci.*, **34**, 1040-1053.
- Chang, E. K. M., and Y. Fu, 2002: Interdecadal variations in Northern Hemisphere winter storm track intensity. *J. Climate*, **15**, 642-658.
- Emori, S., and S. J. Brown, 2005: Dynamic and thermodynamic changes in mean and extreme precipitation under changed climate. Submitted to *Geophys. Res. Lett.*
- Fyfe, J. C., 2003: Extratropical Southern Hemisphere cyclones; Harbingers of climate change? *J. Climate*, **16**, 2802-2805.
- Geng, Q., and M. Sugi, 2003: Possible change of extratropical cyclone activity due to enhanced greenhouse gases and sulfate aerosols—study with a high-resolution AGCM. *J. Climate*, **16**, 2262-2274.
- Hall, N. M. J., B. J. Hoskins, P. J. Valdes, and C. A. Senior, 1994: Storm tracks in a high-resolution GCM with doubled carbon dioxide. *Q. J. R. Meteorol. Soc.*, **120**, 1209-1230.
- Harnik, N., and E. K. M. Chang, 2003: Storm track variations as seen in radiosonde observations and reanalysis data. *J. Climate*, **16**, 480-495.
- Kushner, P. J., I. M. Held, and T. L. Delworth, 2001: Southern Hemisphere atmospheric circulation response to global warming. *J. Climate*, **14**, 2238-2249.
- Lambert, S. J., 1995: The effect of enhanced greenhouse warming on winter cyclone frequencies and strengths. *J. Climate*, **8**, 1447-1452.

- Lee, S., and H.-K. Kim, 2003: The dynamical relationship between subtropical and eddy-driven jets. *J. Atmos. Sci.*, **60**, 1490-1503.
- Lindzen, R. S., and B. F. Farrell, 1980: A simple approximate result for maximum growth rate of baroclinic instabilities. *J. Atmos. Sci.*, **37**, 1648-1654.
- McCabe, G. J., M. P. Clark, and M. C. Serreze, 2001: Trends in Northern Hemisphere surface cyclone frequency and intensity. *J. Climate*, **14**, 2763-2768.
- Meehl, G. A., J. M. Arblaster, and C. Tebaldi, 2005: Understanding future patterns of precipitation extremes in climate model simulations. Submitted to *Geophys. Res. Lett.*
- Min, S.-K., S. Legutke, A. Hense, U. Cubasch, W.-T. Kwon, J.-H. Oh, and U. Schlese, 2005: East Asian climate change in the 21st century as simulated by the coupled climate model ECHO-G under IPCC SRES scenarios. Submitted to *J. Meteor. Soc. Japan*.
- Nakicenovic, N., and R. Swart (eds.), 2000: *Special Report on Emissions Scenarios*. Cambridge University Press, Cambridge, UK, 612 pp.
- Russell, J. L., A. Gnanadesikan, and J. R. Toggweiler, 2005: Impact of westerly wind position on the circulation of the Southern Ocean. Submitted to *J. Climate*.
- Stephenson, D. B., and I. M. Held, 1993: GCM response of northern winter stationary waves and storm tracks to increasing amounts of carbon dioxide. *J. Climate*, **6**, 1859-1870.
- Toggweiler, J. R., J. L. Russell, and S. R. Carson, 2005: The mid-latitude westerlies, atmospheric CO₂, and climate change during the Ice Ages. Submitted to *Paleoceanography*.
- Trenberth, K. E., and D. P. Stepaniak, 2003: Seamless poleward atmospheric energy

transports and implications for the Hadley circulation. *J. Climate*, **16**, 3706-3722.

Figure Captions

Figure 1. The 15-member multi-model ensemble mean of the 2081-2100 minus 1981-2000 zonal mean 2-8 day EKE for (a) DJF and (b) JJA. Contour interval is $3 \text{ m}^2 \text{ s}^{-2}$. The 1981-2000 mean is shown in thick black contours, with a contour interval of $20 \text{ m}^2 \text{ s}^{-2}$. To produce the multi-model ensemble mean of zonal mean 2-8 day EKE, the daily model output is first interpolated to T42 resolution (2.8° by 2.8°) for models with resolution of T42 or higher, and to T21 resolution (5.6° by 5.6°) for models with resolution lower than T42. An 8-day high pass filter is used to produce 2-8 day bandpass-filtered EKE. After the zonal mean is calculated, the results for the lower-resolution models are linearly interpolated in latitude up to T42 resolution, and the multi-model mean is calculated from the zonal means at T42 resolution.

Figure 2. The 15-member multi-model ensemble mean of the 2081-2100 minus 1981-2000 zonal mean of (a,b) temperature, contour interval 1°C ; (c,d) maximum Eady growth rate, contour interval 0.025 day^{-1} ; (e,f) difference in maximum Eady growth rate due to changes in meridional temperature gradient, contour interval 0.025 day^{-1} ; (g,h) difference in maximum Eady growth rate due to changes in static stability, contour interval 0.025 day^{-1} . Thick black contours show 1981-2000 zonal means of (a,b) temperature, contour interval 10°C , with negative contours dashed; (c-h) maximum Eady growth rate, contour interval 0.2 day^{-1} . The left column is DJF, and the right column is JJA. To produce the multi-model ensemble mean, the zonal mean temperature is calculated for each model on the model grid, the zonal means are linearly interpolated in latitude to T42 resolution, and the multi-model mean is calculated from the zonal means at T42 resolution. The

maximum Eady growth rate is calculated from the multi-model mean zonal mean temperature as described in the text.

Figure 3. The 2081-2100 minus 1981-2000 zonal mean for each model of (a,b) 2-8 day EKE vertically integrated from the surface to 200 hPa, units 10^4 J m^{-2} ; (c,d) 2-8 day meridional momentum flux convergence vertically integrated from the surface to 200 hPa, units Pa; (e,f) surface zonal wind stress, units Pa; (g,h) sea level pressure, units hPa; (i,j) precipitation, units mm day^{-1} . The thick black line indicates the multi-model ensemble mean. The left column is DJF, and the right column is JJA. The dots on each line indicate the latitude of the maximum for each variable (except for sea level pressure) for 1981-2000; when the dot is at a latitude where the 2081-2100 minus 1981-2000 difference is increasing towards the pole, there has been a poleward shift in that quantity.

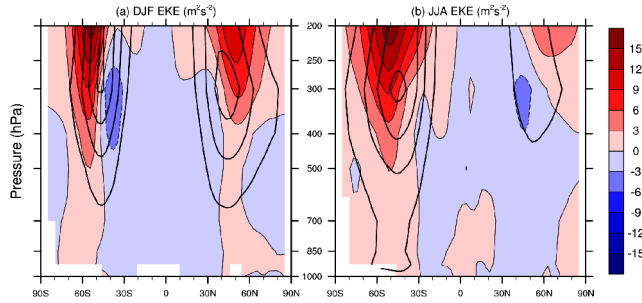


Figure 1. The 15-member multi-model ensemble mean of the 2081-2100 minus 1981-2000 zonal mean 2-8 day EKE for (a) DJF and (b) JJA. Contour interval is $3 \text{ m}^2 \text{ s}^{-2}$. The 1981-2000 mean is shown in thick black contours, with a contour interval of $20 \text{ m}^2 \text{ s}^{-2}$. To produce the multi-model ensemble mean of zonal mean 2-8 day EKE, the daily model output is first interpolated to T42 resolution (2.8° by 2.8°) for models with resolution of T42 or higher, and to T21 resolution (5.6° by 5.6°) for models with resolution lower than T42. An 8-day high pass filter is used to produce 2-8 day bandpass-filtered EKE. After the zonal mean is calculated, the results for the lower-resolution models are linearly interpolated in latitude up to T42 resolution, and the multi-model mean is calculated from the zonal means at T42 resolution.

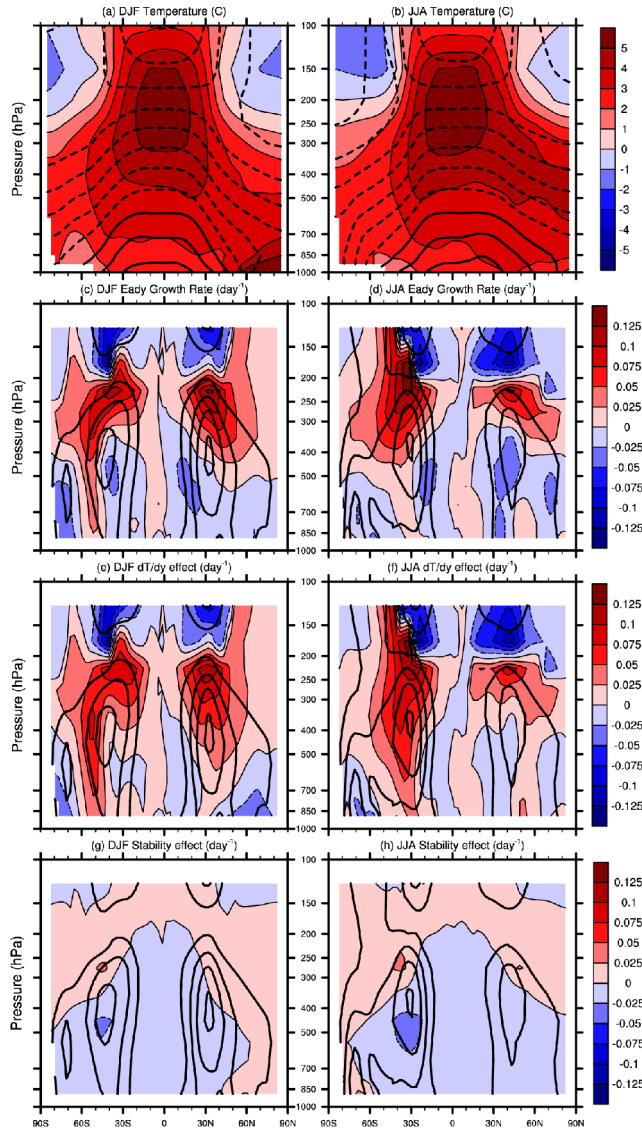


Figure 2. The 15-member multi-model ensemble mean of the 2081-2100 minus 1981-2000 zonal mean of (a,b) temperature, contour interval 1°C ; (c,d) maximum Eady growth rate, contour interval 0.025 day^{-1} ; (e,f) difference in maximum Eady growth rate due to changes in meridional temperature gradient, contour interval 0.025 day^{-1} ; (g,h) difference in maximum Eady growth rate due to changes in static stability, contour interval 0.025 day^{-1} . Thick black contours show 1981-2000 zonal means of (a,b) temperature, contour interval 10°C , with negative contours dashed; (c-h) maximum Eady growth rate, contour interval 0.2 day^{-1} . The left column is DJF, and the right column is JJA. To produce the multi-model ensemble mean, the zonal mean temperature is calculated for each model on the model grid, the zonal means are linearly interpolated in latitude to T42 resolution, and the multi-model mean is calculated from the zonal means at T42 resolution. The maximum Eady growth rate is calculated from the multi-model mean zonal mean temperature as described in the text.

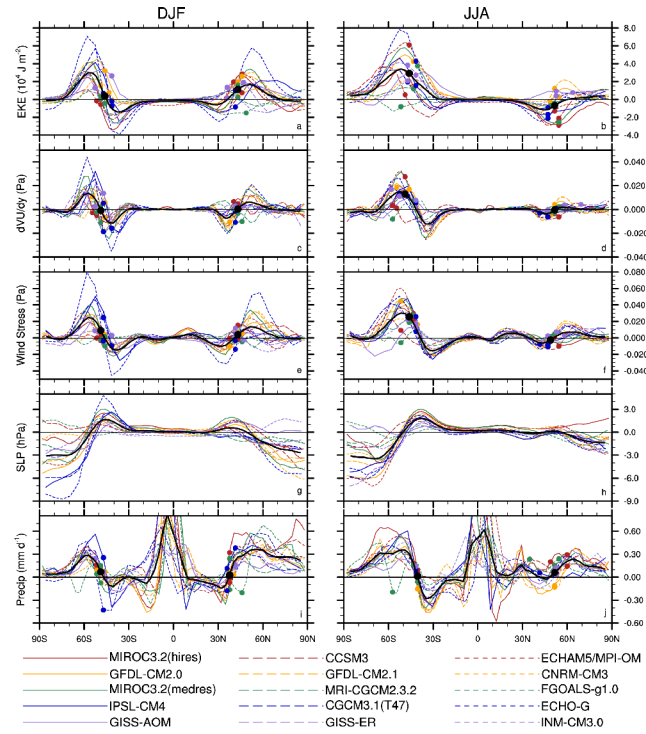


Figure 3. The 2081-2100 minus 1981-2000 zonal mean for each model of (a,b) 2-8 day EKE vertically integrated from the surface to 200 hPa, units 10^4 J m^{-2} ; (c,d) 2-8 day meridional momentum flux convergence vertically integrated from the surface to 200 hPa, units Pa; (e,f) surface zonal wind stress, units Pa; (g,h) sea level pressure, units hPa; (i,j) precipitation, units mm day^{-1} . The thick black line indicates the multi-model ensemble mean. The left column is DJF, and the right column is JJA. The dots on each line indicate the latitude of the maximum for each variable (except for sea level pressure) for 1981-2000; when the dot is at a latitude where the 2081-2100 minus 1981-2000 difference is increasing towards the pole, there has been a poleward shift in that quantity.